*34th EPS Conference on Plasma Phys. Warsaw, 2 - 6 July 2007 ECA Vol.**31F**, P-4.092 (2007)*

Influence of integer *q*-surfaces on the drift of the pellet deposited material

B. Pégourié [(1)], F. Köchl [(2)], H. Nehme [(1)], N. Commaux [(1)], A. Géraud [(1)], L. Garzotti [(3)]

[(1)] *Association Euratom-CEA, CEA/DSM/DRFC, Centre de Cadarache, F-13108 St-Paul-lez-Durance*
[(2)] *Association EURATOM-OEAW/ATI, Kegelgasse 27/3, A-1030 Wien*
[(3)] *Association EURATOM-UKAEA Fusion, Culham Science Centre, UK-OX14 3DB Abingdon*

The ∇B-induced drift of the pellet deposited material plays a crucial role in determining the fuelling efficiency and average depth of the particle source. Owing to its displacement along the magnetic field gradient, the pellet material is deposited deeper into the plasma when the pellet is injected from the High Field Side (as compared to an injection from the Low Field Side), leading to a more efficient fuelling. Up to now, several models were developed for interpreting the experiments and extrapolating present day performance of pellet fuelling to ITER-grade devices [1-3]. Their common feature is that the drift velocity is determined for a part by the balance between (i) a leading term resulting from the compensation of the curvature current by the polarisation current and (ii) a braking term due to an Alfvén wave emission at both ends of the cloud. Conversely, they differ in what concerns the additional braking that is required to reconcile the calculated displacements with the measurements, although all the phenomena invoked up to now originate in the winding of the field lines around the major axis of the machine and specificity of the magnetic configuration. Among them, it is shown in [3] that the different images of the potential distribution resulting from the cloud polarisation overlap when propagating in the plasma. As a consequence, connections appear between the positively and negatively charged parts of the cloud, along which a parallel – resistive – current flows, reducing the cloud polarisation and thus the drift velocity. A first calculation, that neglects the details of the magnetic structure and considers only an average connection length between the positively and negatively charged parts of the cloud, was shown to reproduce satisfactorily the pellet deposition profile in some Tore Supra, JET and FTU experiments [4].

In the model presented here, this approximation is removed and the drift velocity is calculated by taking explicitly into account the variation of the self-connection of the cloud cross-section and of the connection length (i.e. the efficiency of the braking mechanism) as a function of the local value of the safety factor. An example is shown in figures 1*a* and *b* which display a schematic view of the potential distribution around the cloud (figure 1*a*), and the superposition of the images of this potential distribution, in the poloidal plane opposite to that of the cloud, after 7 toroidal turns in each direction (figure 1*b*). The calculation is done at ρ = 0.39 m for parameters typical of Tore Supra: a = 0.75 m, R = 2.4m, magnetic field B_∞ = 4 T, central density and temperature $n_\infty(0)$ = 4 × 10^{19} m^{-3} and $T_\infty(0)$ = 4 keV, safety factor from 0.85 to 3, with a cylindrical cloud of radius R_0 = 1 cm located in the midplane. Although this situation arises a very small time interval after the cloud has been deposited (~1.5 × 10^{-5} s), it can be seen that the different images of the positive and negative parts of the potential distribution overlap in several places, which means that, for a part of the cloud cross-section, there are field lines that connect, through the plasma, regions of opposite polarisation. Since the potential distribution propagates at the Alfvén velocity C_A, the number of toroidal turns to be considered increases with time, proportionally to $C_A t/\pi R$, and thus the proportion of the cloud cross-section P_{con} for which field lines connect regions of opposite polarities.

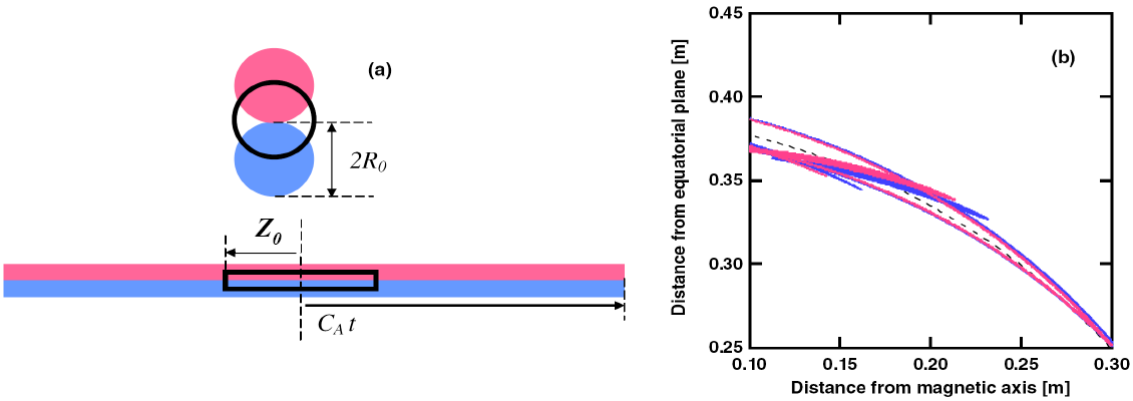

Figure 1. *(a) Diagram of the potential distribution around a cloud cross-section in a poloidal plane and along a flux tube. The region positively (negatively) charged is in red (blue); the over-density itself is limited by the black circle or rectangle and (b) zoom (for a poloidal angle of about π/3 above the equatorial plane) of the cross-section of the plasma showing the superposition of the images of the potential distribution of (a) after 7 toroidal turns in each direction.*

Three regions can be identified on figure 1*b*:
- That without overlap, representing a proportion P_{Alf} of the cloud cross-section, for which the potential propagates along the field lines at the Alfvén velocity. The corresponding damping term is that due to the emission of an Alfvén wave at both ends of the cloud.
- That for which the overlap is such that the connection appears between regions of identical polarisation, leading to a constant potential all along the connecting field lines. No damping is associated with this part of the cloud.
- That, representing a proportion P_{con} of the cloud cross-section, for which the overlap is such that the connection appears between regions of opposite polarisation. In this case, a parallel, resistive current flows along the field lines, decreasing the cloud polarisation and thus the drift of the homogenizing cloud down the magnetic field gradient. This current depends on the value of the parallel electric field, $E_{//}$, and local plasma conductivity $\sigma_{//\infty}$. Its value is $I_{//} = \sigma_{// \infty} E_{//} P_{con} \pi R_0^2$. The relation between $E_{//}$ and $E_\perp$ is obtained from the geometry of the flux tube, whose length is L_{con} and thickness R_0, yielding $E_{//}\left(L_{con} - Z_0\right) \approx E_\perp R_0$.

In addition to $I_{//}$, the currents closing the circuit are the polarisation current in the cloud $I_{pol} = Z_0 R_0 n_0 m_p \dot{E}_\perp / B_\infty^2$, that due to the ∇B and curvature drift $I_{\nabla B} = 2 Z_0 R_0 \left(p_0 - p_\infty\right) / R B_\infty$ and that carried by the Alfvén wave $I_{Alf} = 2 E_\perp P_{Alf} R_0 / \mu_0 C_A$. Using $E_\perp = V_d B_\infty$, the drift velocity V_d is obtained from the condition $\nabla \cdot I = 0$, leading to :

$$\frac{dV_d}{dt} = \frac{2\left(p_0 - p_\infty\right)}{n_0 m_p R} - \frac{V_d B_\infty^2}{n_0 m_p Z_0} \cdot \left[P_{Alf} \frac{2}{\mu_0 C_A} + P_{con} \frac{\pi R_0^2 \sigma_{// \infty}}{L_{con} - Z_0} \right]$$

In these expressions, m_p is the ion mass and $p_{0/\infty}$ are the pressures in the cloud and the plasma, respectively. For times shorter than the time of first connexion τ_{con}, $P_{Alf} = 1$ and $P_{con} = 0$. For longer times, $P_{Alf} \to 0$ and $P_{con} \to 1/2$. The two quantities that govern the magnitude of the damping term due to $I_{//}$ are thus τ_{con} and L_{con}, whose dependence with minor radius ρ is plotted in figures 2*a* and 2*b* for a typical 1 MA Tore Supra discharge.

One sees that integer *q*-surfaces are characterized by small values of τ_{con} and L_{con}, associated to an efficient braking of the drift. In fact, these surfaces act as drift barriers and limit the effective displacement. As a consequence, for a given *q*-profile, the ∇B-induced displacement exhibits a stair-like dependence when plotted versus the pellet penetration, each integer *q*-surface blocking the drift of the pellet deposited material.

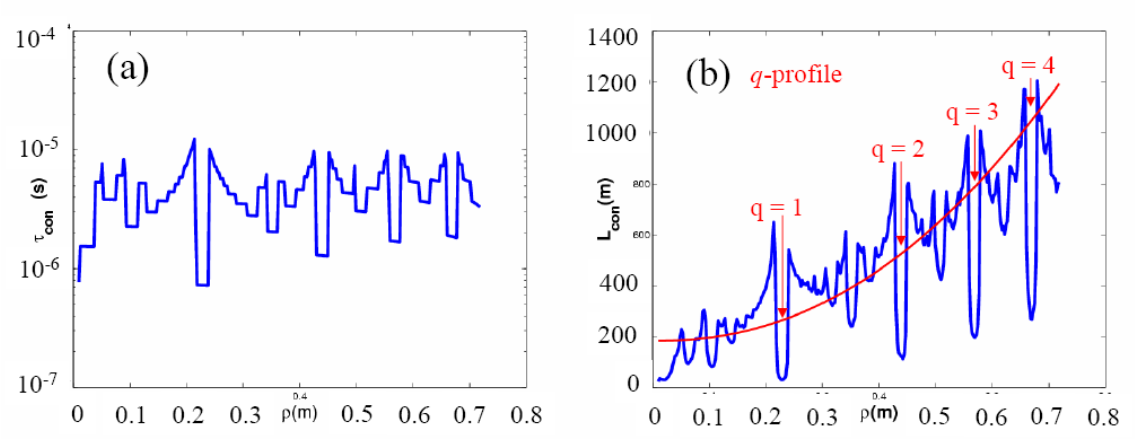

Figure 2. *(a) Time of first connexion, τ_{con}, versus minor radius ρ. (b) Effective connexion length, L_{con}, versus minor radius ρ. The q-profile is also shown.*

Code predictions were compared to a database of about 80 pellets launched from the LFS in Tore Supra ICRH discharges. Main parameters of both the target plasmas and injected pellets are summarized in table 1. Quantities of interest are, for each pellet, the radius of maximum ablation, ρ_{abl}, that of maximum of density increment, ρ_{dep}, and the corresponding values of the safety factor, q_{abl} and q_{dep}. In order to limit the uncertainties due to the fluctuations of the Dα emission, the radius of maximum ablation was estimated from a simple NGS ablation calculation. That of maximum deposition is obtained from the difference between the pre- and post-pellet density profiles, the delay between the time at which the pellet is injected and that at which the post-pellet density is measured being in all cases less than 5 ms. In each case, the corresponding value of the safety factor is taken from equilibrium reconstruction.

I_p [MA]	$n_\infty(0)$ [10^{19} m^{-3}]	$n_\infty(a)$ [10^{19} m^{-3}]	$T_\infty(0)$ [keV]	$T_\infty(a)$ [keV]	$q(a)$	V_p [m/s]	N_p [10^{20} D]
0.6	5.2	1.9	2.3	0.18	8	200 - 240	2.6 - 4
1	4.4	0.9	4.1	0.7	4.6	190 - 200	1.8 - 4
1.3	5.2	0.95	4.1	0.56	3.5	100 - 200	3.2 - 5

Table 1. *Main parameters of the target plasmas for the database of LFS-launched pellets used in the present study. Plasma current, I_p, central and edge densities and temperatures, $n_\infty(0/a)$ and $T_\infty(0/a)$, edge safety factor, $q(a)$ and pellet injection velocity and particle content, V_p and N_p. In all cases, the magnetic field is $B_\infty = 3.7$ T and the ICRH power $P_{ICRH} = 4.5$ MW.*

No substructure appears when ρ_{dep} is plotted versus ρ_{abl} for the whole database (I_p = 0.6, 1 and 1.3 MA, figure 3*a*): the points are uniformly distributed over the whole interval with an average value of the displacement $(\rho_{dep} - \rho_{abl}) \approx 7$ cm. Conversely, for I_p = 1 MA, the ρ_{dep}'s tend to cluster around ~ 0.54×a for $\rho_{abl} < 0.55\times a$ and ~ 0.72×a for $\rho_{abl} > 0.55\times a$, these values of ρ_{dep} corresponding approximately to the location of q = 2 and q = 3 (figure 3*b*). This behaviour can be generalized to the whole database. This is displayed in figure 3*c*, where q_{dep} is plotted versus q_{abl} for the three groups of pellets (I_p = 0.6, 1 and 1.3 MA). In this case also, the q_{dep}'s cluster around 2 or 3, depending on whether q_{abl} is smaller or larger than ~ 2. The results of the corresponding simulations are displayed in figure 3*d*, exhibiting

the same trend. This good agreement between measurements and code predictions strongly supports the model described in the first part of the paper. Nevertheless, it is found that the values of the global displacement calculated by this way are not significantly different to those found when neglecting the effect of rational *q*-values. It follows that the calculation described in [3] seems to be accurate enough for any practical purpose.

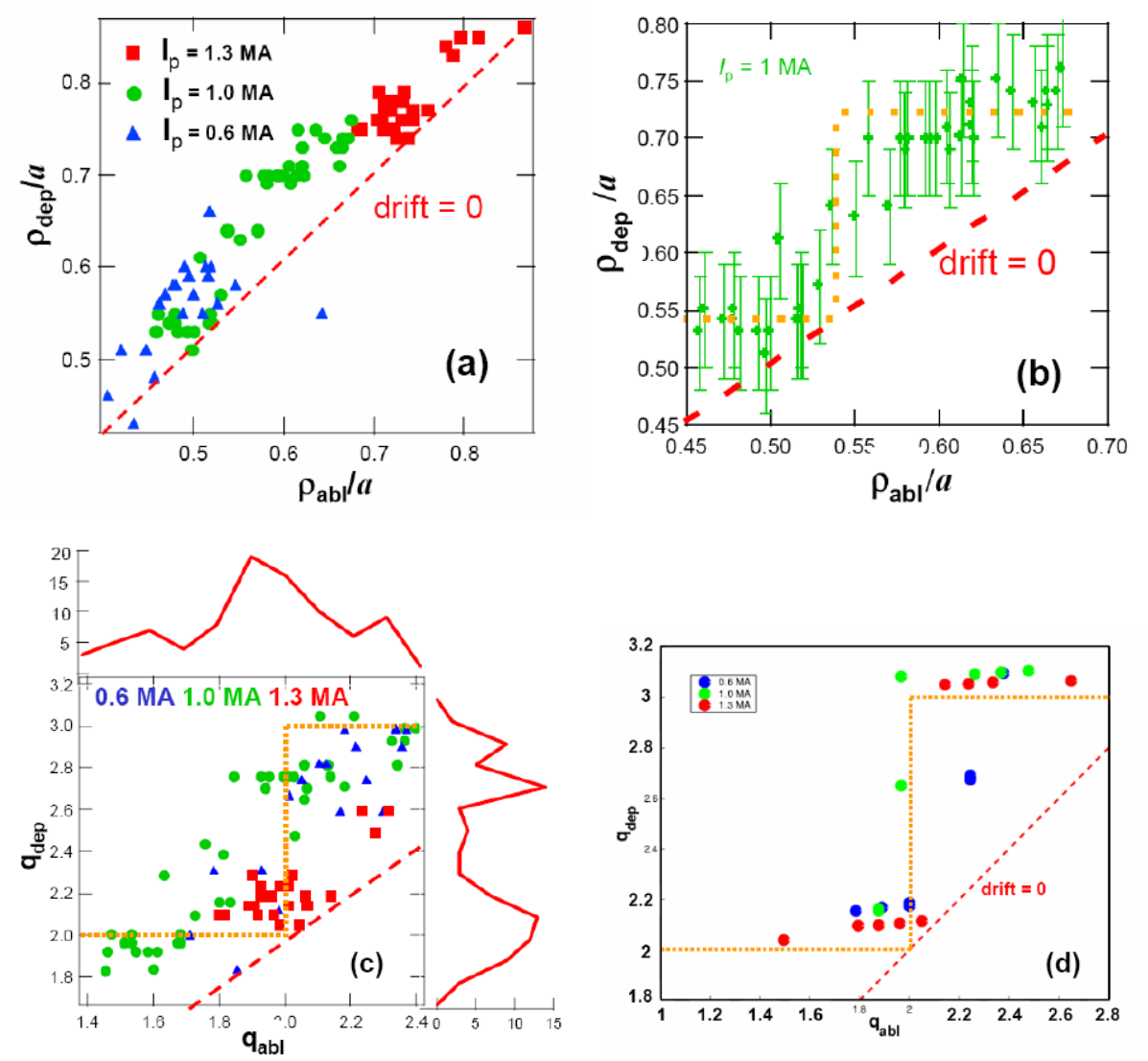

Figure 3. *(a) ρ_{dep}/a versus ρ_{abl}/a for pellets launched from the LFS in I_p = 0.6, 1 and 1.3 MA.*
(b) Indentical to (a) for pellets launched in I_p = 1 MA discharges. Yellow dotted lines are the position of the q_{dep} ; q_{abl} = 2 and q_{dep} = 3 flux surfaces.
(c) q_{dep} versus q_{abl} for the whole database. Red curves are histograms showing the two components of the distribution of q_{dep} when the q_{abl}'s are uniformly distributed between 1.5 and 2.5.
(d)Simulated counterpart of (c).

References

[1] P.B. Parks *et al.*, Phys. Rev. Lett. **94** (2005) 125002
[2] I. Yu. Senichenkov *et al.*, Nucl. Fusion **46** (2006) 788
[3] B. Pégourié *et al.*, Nucl. Fusion **47** (2007) 44
[4] A. Géraud *et al.*, ECA **Vol. 27A**, EPS (2003) P-1.97
F. Köchl *et al.*, **Pellet Drift Effect Studies at JET**, this conference
D. Terranova *et al.*, Nucl. Fusion **47** (2007) 288